THE ASTROPHYSICAL JOURNAL, 489:L75–L78, 1997 November 1
© 1997. The American Astronomical Society. All rights reserved. Printed in U.S.A.

HUBBLE SPACE TELESCOPE OBSERVATIONS OF THE MIDDLE-AGED PULSAR 0656+14

G. G. PAVLOV
Department of Astronomy and Astrophysics, Pennsylvania State University, 525 Davey Lab, University Park, PA 16802; pavlov@astro.psu.edu
A. D. WELTY
Computer Sciences Corporation, Space Telescope Science Institute, 3700 San Martin Drive, Baltimore, MD 21218; welty@stsci.edu
AND
F. A. CÓRDOVA
Department of Physics, University of California, Santa Barbara, Santa Barbara, CA 93106; cordova@omni.ucsb.edu
Received 1997 July 14; accepted 1997 August 22; published 1997 October 1

ABSTRACT

Multiwavelength spectral observations of middle-aged ($\tau \sim 10^4$–10^6 yr) isolated pulsars enable one in principle to separate thermal radiation emitted from the neutron star surface and nonthermal radiation from its magnetosphere. We have previously detected the middle-aged radio and soft X-ray pulsar 0656+14 with the *Hubble Space Telescope* Faint Object Camera (FOC) long-pass filter F130LP. In the present Letter we report new FOC observations of this pulsar with three broadband filters: F430W, F342W, and F195W. The optical-UV spectral flux can be fitted with a two-component spectral model that combines a power-law spectrum with a Rayleigh-Jeans spectrum. The nonthermal component with the power-law index $\alpha = 1.4^{-0.7}_{+0.6}$ dominates at $\lambda \gtrsim 3000$ Å. The thermal component is characterized by the Rayleigh-Jeans parameter, $G \equiv T_6(R_{10}/d_{500})^2$, where $T = 10^6 T_6$ K is the brightness temperature, $R_\infty = 10R_{10}$ km is the neutron star radius as seen by a distant observer, and $d = 500d_{500}$ pc is the distance. For a plausible extinction, $E(B-V) = 0.03$, we obtained $G = 3.6^{+1.6}_{-2.0}$. The observed shape of the optical-UV spectrum of PSR 0656+14 differs drastically from those of both younger pulsars (Crab, 0540−69, Vela) and the older pulsar Geminga.

Subject headings: pulsars: general — pulsars: individual (PSR 0656+14) — stars: atmospheres — stars: evolution — stars: interiors — stars: neutron

1. INTRODUCTION

The best candidates for investigation of neutron star (NS) cooling, which depends essentially on still poorly known properties of the superdense matter in NS interiors, are middle-aged ($10^4 \lesssim \tau \lesssim 10^6$ yr) NSs whose surface temperatures are expected to be in the range of 10^5–10^6 K. Soft X-ray observations of middle-aged pulsars revealed that at least three of them, PSR 0656+14, Geminga, and PSR 1055−52 (τ = 1.1, 3.4, and 5.3×10^5 yr, respectively), emit thermal radiation with blackbody temperatures of $\sim(3\text{–}10) \times 10^5$ K (Ögelman 1995). However, interpretation of these observations is not completely certain—for instance, fitting the observed spectra with hydrogen atmosphere models (Pavlov et al. 1995) yields systematically lower effective temperatures (by a factor of 1.5–2.5, depending on the magnetic field) than the traditional blackbody fits. Such a difference in temperatures corresponds to quite different cooling scenarios and different models of the NS interiors. To evaluate the effective temperature firmly, it is important to investigate the NS thermal radiation in the UV-optical range (Pavlov et al. 1996b). Although the nonthermal component could dominate in the optical spectrum of middle-aged pulsars, the thermal flux grows with frequency and is expected to dominate in the UV domain. Since predicted UV fluxes are extremely faint, and the most promising far-UV range is unobservable from the ground, the *Hubble Space Telescope* (*HST*) is most suitable for such observations.

Indeed, the first *HST* observations of the middle-aged pulsars proved to be successful. Pavlov, Stringfellow, & Córdova (1996a, hereafter PSC96) detected PSR 0656+14 with the Faint Object Camera (FOC) in the long-pass filter F130LP ($\lambda\lambda$ = 2310–4530 Å at half-maximum) and showed that the pulsar flux in this filter is mainly of nonthermal origin, perhaps with a contribution from the thermal component. Mignani, Caraveo, & Bignami (1997a) observed the same pulsar with the Wide Field Planetary Camera (WFPC2) in the wide-band F555W filter ($\lambda\lambda$ = 4600–6200 Å) and confirmed marginal detection of this pulsar in the *V* band with ground-based telescopes (Caraveo, Bignami, & Mereghetti 1994). The soft X-ray and γ-ray pulsar Geminga has been observed in several UV-optical spectral bands (Bignami et al. 1996, and references therein). Its spectrum was interpreted as a superposition of thermal and nonthermal components, with an apparent emission line at $\lambda \approx 6000$ Å. Finally, PSR 1055−52 has likely been detected in the FOC F342W filter (Mignani, Caraveo, & Bignami 1997b), although observations with more filters would be needed to confirm this detection.

The goal of our new *HST* FOC observations reported here was to measure the fluxes from PSR 0656+14 in several bands, particularly in the UV domain. We chose the FOC filters F430W, F342W, and F195W, which cover the range $\lambda\lambda \sim$ 1700–4500 Å. Supporting ground-based *BVRI* observations were made at the 6 m telescope of the Russian Academy of Sciences (Kurt et al. 1997).

2. OBSERVATIONS AND DATA REDUCTION

Our observations of PSR 0656+14 (1996 March 24) consist of two exposures in each of five satellite orbits. Three FOC/96 filters were used: F342W for one orbit (two exposures), F430W for one orbit (two exposures), and F195W for three orbits (six exposures). The point-spread function (PSF) of one of the F195W exposures has an anomalously large width and correspondingly low amplitude. That exposure has been removed from consideration. We have also reanalyzed the WFPC2 F555W archive data (observations of 1996 January 18, by Mignani et al. 1997a).

Processing and analysis of the data made use of standard

TABLE 1

HST OBSERVATIONS OF PSR 0656+14

Filter	Pivot λ (Å)	Exposure (s)	Source[a] (counts)	Sky[b] (counts pixel^{-1})	S/N	Net[c] (counts)	Count Rate (counts s^{-1})	Flux[d]
F195W[e]	2360	6102[g]	497 ± 47	4.26	10.6	628	0.103 ± 0.010	0.349 ± 0.043
F342W[e]	3402	2243[h]	431 ± 35	1.89	12.3	510	0.227 ± 0.018	0.307 ± 0.027
F430W[e]	4117	2434[h]	339 ± 35	2.25	9.7	396	0.163 ± 0.017	0.264 ± 0.029
F555W[f]	5443	6200[i]	613 ± 27	13.2	22.6	697	0.112 ± 0.005	0.388 ± 0.038

[a] Background-subtracted source counts with 1 σ uncertainties using an $r = 8$ pixel aperture for FOC and an $r = 5$ pixel aperture for WFPC2.

[b] Total (sky plus dark noise) median background for summed exposure.

[c] Source counts incorporating encircled energy corrections based on PSF.

[d] Mean energy flux F_ν in units of 10^{-29} ergs cm^{-2} s^{-1} Hz^{-1}; systematic uncertainties are included.

[e] FOC/96 observations.

[f] WFPC2 observations.

[g] Sum of five exposures.

[h] Sum of two exposures.

[i] Sum of eight exposures.

IRAF and STSDAS tools. We co-added the F342W, F430W, and remaining five F195W exposures into three filter-specific images. The only obvious source in these 7.″4 × 7.″4 images has coordinates $\alpha_{2000} = 6^h59^m48^s.106$, $\delta_{2000} = 14°14'20''.33$ (measured from the F342W and F430W images, for which the filter-induced shifts are known; nominal accuracy is 0.″01–0.″02). The expected radio position of the pulsar for the epoch of our observation can be found with the aid of previous Very Large Array and timing observations (see PSC96 for references): $\alpha_{2000}(1996.23) = 6^h59^m48^s.149 \pm 0^s.007$, $\delta_{2000}(1996.23) = 14°14'21''.23 \pm 0''.04$; our FOC position is offset from this point by 1.″10 (vs. 0.″67 in the FOC observation of PSC96). If we calculate the expected position based on the FOC observation of PSC96 (epoch 1994.13) and the radio proper motion ($\mu_\alpha = +0''.073 \pm 0''.020$ yr^{-1}, $\mu_\delta = -0''.026 \pm 0''.013$ yr^{-1}; see Thompson & Córdova 1994; PSC96), the expected position is $\alpha_{2000}(1996.23) = 6^h59^m48^s.103$ and $\delta_{2000}(1996.23) = 14°14'21''.23$, so that the offset is 0.″90. On the other hand, there is no doubt that the object we observed is indeed the optical counterpart of PSR 0656+14—it follows from the upper limit for undetected sources (PSC96), and it was directly proven by observation of pulsations of this object in the *B* band (Shearer et al. 1996). Thus, we have to conclude that the combined accuracy of the guide star positions and FOC aperture pointing is limited by ∼1″ (cf. PSC96).

We performed aperture photometry to determine the number of source counts in each filter. The measured energy fraction ϵ, required for correction of measured count rates, is not tabulated in the FOC Instrument Handbook (FIH) for any of our filters. We estimated it as follows. Our target is nearly centered in the 512 × 512 pixel field of view, and there are no other obvious sources. This allowed us to use a large annulus (inner and outer radii of 70 and 140 pixels, respectively) to measure and subtract the sky background. We measured the target counts for apertures with radii from 2 to 30 pixels. Plots of counts versus aperture for the F342W and F430W filters are very similar to those for similar wavelength FOC filters, whose data are in the FIH. This includes a general flattening near $r = 15$ pixels. We chose to take the measurements in apertures of radius $r = 8$ pixels because the flattening has begun by then and there is much less sensitivity to the background uncertainty than when using larger radii. Interpolating the FIH ϵ table values, we find that 85% and 86% of the source counts are probably included within that radius in the F342W and F430W data, respectively. The F195W counts versus radius curve rises more slowly than that for other filters of similar wavelength, which indicates a somewhat broader PSF for our data. For consistency, we used an $r = 8$ pixel aperture, for which we estimate $\epsilon = 0.79$.

Although the F195W source counts do level off near $r = 15$ pixels, they rise significantly at larger radii. We think this is due to a low spatial frequency nonuniformity in the background, which may be due to poor flat-fielding or possibly real background structure. There is no standard F195W flat field with which to reprocess the data. We did reprocess the data with flat fields other than the one recommended, but results were worse, as expected.

We converted the source counts to the mean fluxes, $\bar{F}_\nu$, as described in PSC96. The count rate errors presented in Table 1 are statistical errors based on signal-to-noise ratios (S/Ns) calculated in a standard way (see FIH). Actual uncertainties of the measured fluxes include systematic errors associated with the flat-fielding, encircled energy corrections (which depend on the actual shape of the PSF), and uncertainties of the detector quantum efficiency. We estimated probable total systematic uncertainties of ≃10%, 7%, and 6% for F195W, F342W, and F430W, respectively, and added the corresponding errors in quadrature to the statistical errors. The resulting total uncertainties for the mean fluxes are given in Table 1.

The "counts" for the WFPC2/F555W filter in Table 1 are the CCD Data Numbers (DN) obtained with the gain of 7 e^-/DN. The source "counts" were extracted from the circle of 5 pixel (0.″23) radius ($\epsilon = 0.88$). The mean flux we obtained exceeds that reported by Mignani et al. (1997a) by ≃13%. Since DN statistics are not Poissonian, we converted the "counts" to photoelectrons to evaluate the statistical noise (which includes background noise and CCD read noise) and the S/N. We added a systematic uncertainty of 4% to the statistical error to estimate the total uncertainty (≃10%) of the F555W flux value.

3. DISCUSSION

The mean fluxes of the PSR 0656+14 counterpart in the F430W, F342W, F195W, and F555W bands are shown in Figure 1, together with the FOC F130LP flux (PSC96) and the *B*, *V*, *R*, and *I* fluxes (Kurt et al. 1997). We see that the flux decreases with increasing frequency (approximately as $\nu^{-1.4}$) in the *I*–*V* range and apparently starts growing at $\lambda \lesssim 4000$ Å. This behavior firmly confirms a nonthermal origin for the optical radiation and indicates that a thermal component from the NS

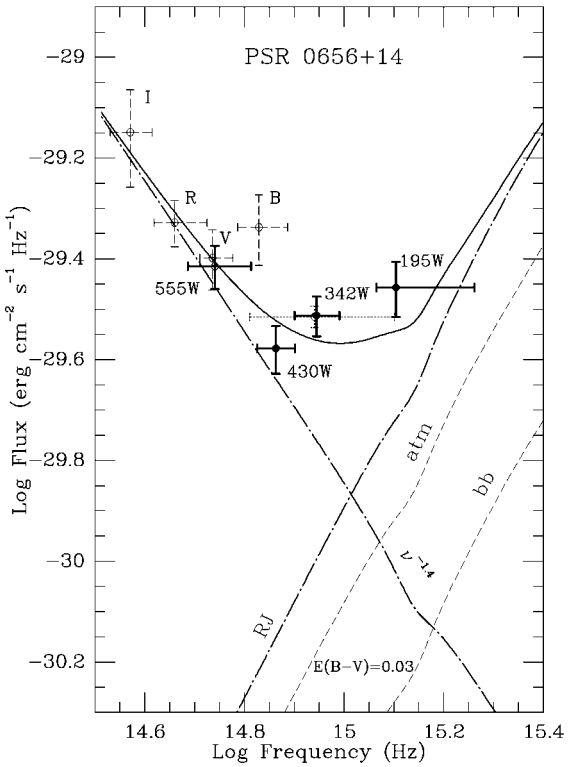

FIG. 1.—Fluxes observed from the PSR 0656+14 optical counterpart in different spectral bands. The heavy solid crosses 430W, 342W, and 195W show results of our last *HST* FOC observations; 555W marks the flux obtained from WFPC2 observations of Mignani et al. (1997a). The flux detected by PSC96 with the FOC F130LP filter is shown with the dotted cross; the dashed crosses *B*, *V*, *R*, and *I* show the corresponding fluxes measured with the 6 m telescope (Kurt et al. 1997). The solid curve shows the best fit of the fluxes in the nine bands with the two-component model (power law plus Rayleigh-Jeans spectrum; eq. [1]) for the color excess $E(B-V) = 0.03$. The dash-dotted lines are the components of this model. The dashed lines labeled "bb" and "atm" are obtained by fitting the thermal soft X-ray *ROSAT* spectrum with the blackbody model and NS atmosphere model.

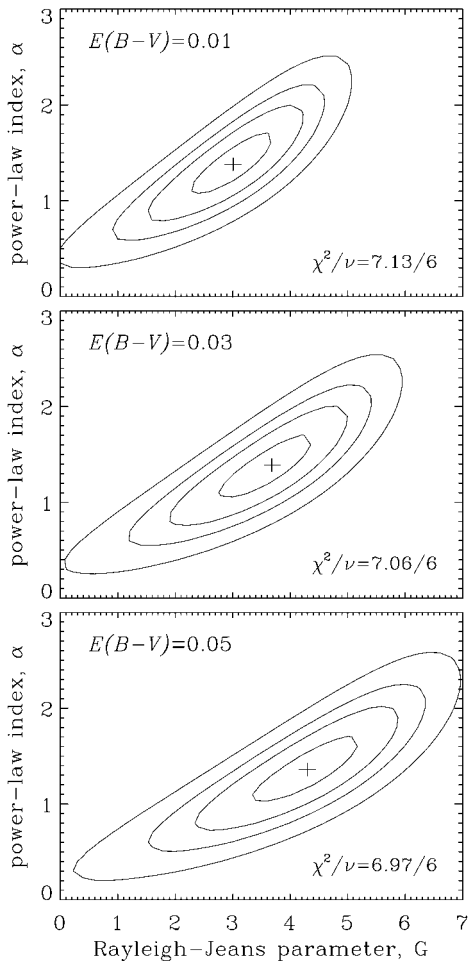

FIG. 2.—Confidence levels (20%, 68%, 90%, and 99%) for the two-component fits (eq. [1]) of the observed spectrum of PSR 0656+14 at three values of the color excess $E(B-V)$.

surface becomes perceptible in the UV part of the spectrum (PSC96). Parameters of the thermal and nonthermal fluxes can be constrained by fitting the observed spectrum with a two-component model (cf. PSC96; Kurt et al. 1997), a sum of the power-law and thermal spectra (the latter has the form of a Rayleigh-Jeans spectrum at these frequencies for plausible NS temperatures):

$$f(\nu) = \left[f_0 \left(\frac{\nu}{\nu_0}\right)^{-\alpha} + g_0 \left(\frac{\nu}{\nu_0}\right)^2 \right] \times 10^{-0.4A(\nu)}, \qquad (1)$$

where ν_0 is an arbitrary reference frequency (we chose $\nu_0 = 8.766 \times 10^{14}$ Hz, which corresponds to $\lambda_0 = 3420$ Å), $A(\nu)$ is the interstellar extinction (see, e.g., Savage & Mathis 1979), and f_0 and g_0 are the values of the nonthermal and thermal fluxes at $\nu = \nu_0$. The coefficient g_0 can be expressed in terms of the (apparent) NS brightness temperature $T = 10^6 T_6$ K, NS radius (as seen by a distant observer) $R_\infty = 10R_{10}$ km, and distance $d = 500 d_{500}$ pc to the pulsar: $g_0 = 3.12 \times 10^{-31} G$ ergs cm^{-2} s^{-1} Hz^{-1}, and $G \equiv T_6 (R_{10}/d_{500})^2$. According to PSC96, a plausible value for the color excess, which determines the extinction curve $A(\nu)$, is $E(B-V) = 0.01$–0.05 ($A_V = 0.03$–0.15). We fitted the fluxes in the nine bands with equation (1) for $E(B-V) = 0.01$, 0.03, and 0.05, varying f_0, α, and G. The best-fit models (minimum $\chi^2 = 7.13$, 7.06, and 6.97 for 6 degrees of freedom) correspond to $f_0 = 0.19$, 0.20, and 0.21 μJy, $\alpha = 1.4$, 1.4, and 1.4, and the Rayleigh-Jeans parameter $G = 3.0$, 3.7, and 4.3. The best-fit spectrum for $E(B-V) = 0.03$ and its components are shown in Figure 1.

Figure 2 shows confidence regions for our fits in the G-α plane. These regions are considerably narrower than those obtained by Kurt et al. (1997) without the new FOC observations reported here. Varying the color excess within the plausible limits has almost no effect on the power-law index, whereas the boundaries of the Rayleigh-Jeans parameter shift to higher values with increasing $E(B-V)$.

The values of G obtained from our fits can be compared with what is expected from extrapolations of the soft X-ray spectral flux observed with the *ROSAT* and *ASCA* (Finley, Ögelman, & Kiziloğlu 1992; Anderson et al. 1993; Greiveldinger et al. 1996) to the optical range. The result of this extrapolation depends on the model used for fitting the X-ray spectrum. The blackbody fit of the *ROSAT* spectrum yields $T_6 = 0.9 \pm 0.04$ for $R_{10}/d_{500} = 1.0 \pm 0.2$ (Finley et al. 1992), which corresponds to the Rayleigh-Jeans parameter $G = 0.9 \pm 0.3$. A fit of the same data with a set of hydrogen NS atmosphere models (Pavlov et al. 1995) gives, for $B = 4.7 \times 10^{12}$ G, the radius-to-distance ratio $R_{10}/d_{500} = 2.3 \pm 0.4$ and the *effective* temperature $T_\infty^{\rm eff} = (5.3 \pm 0.5) \times 10^5$ K

(Anderson et al. 1993). Since the model spectrum differs from the blackbody spectrum, there is no universal relation between the effective and brightness temperatures. However, the model spectrum in the optical range can be fitted with the Rayleigh-Jeans spectrum with $T \simeq 0.9T_{\infty}^{\rm eff}$, giving $G \simeq 2.6 \pm 0.7$. Another set of *ROSAT*+*ASCA* data was fitted by Greiveldinger et al. (1996) with a three-component model (soft and hard blackbodies and a power law), which presumably represent the whole NS surface, a polar cap, and nonthermal radiation. Of the first two, only the soft blackbody component, with $T_6 = 0.78^{+0.05}_{-0.14}$, can be observed in the optical-UV range. The corresponding radius-to-distance ratio, $R_{10}/d_{500} \simeq 1.6^{+0.8}_{-0.1}$, can be estimated from the soft component bolometric flux (Table 2 of that paper); it yields $G = 2.1^{+1.6}_{-0.2}$. This range strongly overlaps with that obtained for the atmosphere model fit. However, it was derived from a different data set and is too broad because it was obtained from the three-component model with strongly correlated parameters.

Comparing the G values inferred from our fits with those obtained from the soft X-ray fits by Finley et al. (1992) and Anderson et al. (1993), we see that the latter shows a better agreement. However, it implies a distance to the pulsar, $d \simeq 280R_{13}$ pc ($R_{\infty} = 13$ km corresponds to "canonical" values of the NS mass and radius, $M = 1.4\ M_{\odot}$, $R = 10$ km), that is much smaller than the $d \simeq 760$ pc estimated from the radio pulsar dispersion measure, 14 cm^{-3} pc. (Moreover, the *ROSAT* PSPC response matrix was poorly known when the fits of Anderson et al. were obtained; a corrected response yields even smaller distances.) The small distance is consistent with similar (albeit not very certain) values of the hydrogen column densities, $n_{\rm H} \sim (0.5\text{–}2) \times 10^{20}$ cm^{-2}, estimated from soft X-ray observations of PSR 0656+14 (see the papers cited above) and Geminga (see, e.g., Halpern, Martin, & Marshall 1997), whose position on the celestial sphere is close to that of 0656+14 and whose distance is 157^{+59}_{-34} pc, as obtained by Caraveo et al. (1996) by measuring Geminga's parallax. On the other hand, radio pulsations of Geminga show a much lower dispersion measure, 3 cm^{-3} pc (Kuzmin & Losovsky 1997), i.e., much lower electron column density (9×10^{18} vs. 4×10^{19} cm^{-2}), in agreement with the larger distance to 0656+14 determined from the dispersion measure. Since the radio dispersion is measured with higher accuracy than $n_{\rm H}$, we cannot exclude that 0656+14 is indeed at $d \sim 700$ pc and does not have a hydrogen atmosphere (which is not surprising for an active young pulsar); then the close values of the Rayleigh-Jeans parameter is a chance coincidence. On the other hand, for $d = 760$ pc, the best-fit G yields $T = 5 \times 10^6 R_{13}^{-1}$ K. Such a brightness temperature appears to be too high for a pulsar of the characteristic age 1.1×10^5 yr unless the radiation at optical-UV frequencies emerges from layers with temperature considerably higher than $T^{\rm eff}$.

Although the slope of the nonthermal spectrum is not strongly constrained because of relatively large errors (especially in the I band), it looks much steeper than those of the (much younger) Crab pulsar, $\alpha = -0.11 \pm 0.13$ (Percival et al. 1993; see also Ransom et al. 1994), and PSR 0540−69, $\alpha \simeq 0.2$ (Nasuti et al. 1997). The nonthermal component of the younger Vela pulsar has the slope $\alpha \simeq 0.3$ in the *VBU* range, but, according to Nasuti et al. (1997), its R flux is about half the value obtained from extrapolation of the power law. Even more drastic difference is seen between the shapes of the optical spectra of PSR 0656+14 and the older pulsar Geminga, which looks very much like 0656+14 in the soft X-ray range. Geminga's flux has a minimum at the B band, peaks at the V band, and falls off sharply redward. On the contrary, the flux of 0656+14 grows redward of V, demonstrating that the properties of the nonthermal IR-optical-UV radiation are not the same in different pulsars and do not have a clear correlation with the pulsar age.

The measured mean fluxes (Fig. 1) show a nonmonotonic behavior at $\lambda\lambda \sim 4000$–5000 Å: an excess in the B band and a deficit in the F430W band, with a difference of $\simeq$0.6 mag. This indicates that a spectral feature might be present at these wavelengths. Its statistical significance, however, is marginal. Besides, the B and F430W fluxes were obtained with different instruments at different telescopes and different times. We cannot exclude that the difference is due to an unknown systematic error of one of the instruments or that the nonthermal component may vary with time. We believe that more observations (preferably simultaneous, and with the same instrument) are needed to verify whether the feature is real.

This work was partially supported by NASA through grant GO-06645.01-95A from the Space Telescope Science Institute, which is operated by the Association of Universities for Research in Astronomy, Inc., under NASA contract NAS 5-26555, and through NASA grant NAG5-2807. We thank Slava Zavlin for his help with computing NS atmosphere models.

REFERENCES

Anderson, S. B., Córdova, F. A., Pavlov, G. G., Robinson, C. R., & Thompson, R. J. 1993, ApJ, 414, 867
Bignami, G. F., Caraveo, P. A., Mignani, R., Edelstein, J., & Bowyer, S. 1996, ApJ, 456, L111
Caraveo, P. A., Bignami, G. F., & Mereghetti, S. 1994, ApJ, 422, L87
Caraveo, P. A., Bignami, G. F., Mignani, R., & Taff, L. G. 1996, ApJ, 461, L91
Finley, J. P., Ögelman, H., & Kiziloğlu, Ü. 1992, ApJ, 394, L21
Greiveldinger, C., et al. 1996, ApJ, 465, L35
Halpern, J. P., Martin, C., & Marshall, H. L. 1997, ApJ, 473, L37
Kurt, V. G., Sokolov, V. V., Zharikov, S. V., Pavlov, G. G., & Komberg, B. V. 1997, A&A, submitted
Kuzmin, A. D., & Losovsky, B. Y. 1997, IAU Circ., 6559
Mignani, R., Caraveo, P. A., & Bignami, G. F. 1997a, Messenger, 87, 43
———. 1997b, ApJ, 474, L51
Nasuti, F. P., Mignani, R., Caraveo, P. A., & Bignami, G. F. 1997, A&A, 323, 839
Ögelman, H. 1995, in The Lives of the Neutron Stars, ed. A. Alpar, Ü. Kiziloğlu, & J. van Paradijs (Dordrecht: Kluwer), 101
Pavlov, G. G., Shibanov, Yu. A., Zavlin, V. E., & Meyer, R. D. 1995, in The Lives of the Neutron Stars, ed. A. Alpar, Ü. Kiziloğlu, & J. van Paradijs (Dordrecht: Kluwer), 71
Pavlov, G. G., Stringfellow, G. S., & Córdova, F. A. 1996a, ApJ, 467, 370 (PSC96)
Pavlov, G. G., Zavlin, V. A., Trümper, J., & Neuhäuser, R. 1996b, ApJ, 472, L33
Percival, J. W., et al. 1993, ApJ, 407, 276
Ransom, S. M., Fazio, G. G., Eikenberry, S. S., Middleditch, J., Kristian, J., Hays, K., & Pennypacker, C. R. 1994, ApJ, 431, L43
Savage, B. D., & Mathis, J. S. 1979, ARA&A, 17, 73
Shearer, A., et al. 1996, IAU Circ., 6502
Thompson, R. J., & Córdova, F. A. 1994, ApJ, 421, L13